STUDIA UBB CHEMIA, LVII, 3, 2012 (p. 167 – 176)
(RECOMMENDED CITATION)

# HOW PLASMA SPECIES AFFECT THE STRUCTURAL AND MORPHOLOGICAL PROPERTIES OF MWCNTS

**SOMAYEH SHAMS[1, *], ZAHRA KHALAJ[1], MAHMOOD GHORANNEVISS[1]**

**ABSTRACT.** Multi wall carbon nanotubes have been synthesized by DC-Plasma Enhanced Chemical Vapor Deposition with different plasma species. $N_2$ and Ar were added individually to the mixture of $C_2H_2/H_2$ plasma in the growth step of CNTs synthesis. The effect of plasma on pretreatment of catalyst film was studied as well as its effects on the CNTs diameter, structural quality and growth density, as given by Raman spectroscopy and Scanning Electron Microscopy. Special feature of this work is the use of gold as catalyst over Ni substrate. The results indicate that using $N_2/C_2H_2/H_2$ plasma, the diameter size of the CNTs in comparison with $C_2H_2/H_2$ plasma was increased whereas structural quality of these samples is the same. Conversely, using $Ar/C_2H_2/H_2$ plasma, a considerable decrease in the diameter size and quality of the CNTs was observed.

***Keywords:*** *Plasma CVD, nanotubes, Hydrogen etching, Gold catalyst.*

## INTRODUCTION

Carbon nanotubes (CNTs) synthesis based on CVD methods involves the catalytic decomposition of a carbon precursor on the substrate [1]. Transition metals such as Fe, Co, Ni, Mo, etc. [2-6] have been used as catalyst for CNTs growth in most of the researches and synthesis parameters for CNTs growth over these catalysts have been widely studied [7-15]. Studies have shown gold (Au) in nanometer scale with catalytic properties, in addition to photo catalytic properties; it has attracted considerable researches in biomedical [16-23] and imaging filed [24, 25]. On the other hand, applications of CNTs in technologies such as field-emission devices, nanolithography, ballistic transistors, X-ray generators, gas sensors [26-31] are well known nowadays. Due to the scale, structure and biocompatibility of CNTs, considerable attention was paid in biomedical applications, such as drug delivery, cancer therapy, imaging and diagnostics [32,33]. It is expected that, in the CNTs tip-growth mode [34, 35] over the Au catalyst, CNT tops be ended by Au nanoparticles. This combination CNT/Au would be attractive for biomedical applications.

[1] *Plasma Physics Research Center, Science and Research Branch, Islamic Azad University, Tehran, Iran*
[*] *Correspondent: somayehshamss@gmail.com*

After discovery of CNTs, by Iijima in 1991 [36] by arc discharge in the helium atmosphere, several methods have been developed for CNTs synthesis. The main methods are: arc discharge, laser ablation and several types of CVD. Among these last methods, Plasma CVD is applied widely for synthesizing carbon nanotubes and other carbon nanostructures [37,38]. Electrical field of plasma makes the grown structures well aligned, with high quality, in lower temperature comparison to other methods; plasma enhanced PECVD is a controllable and predefined method in this respect. Therefore, we used a home made PECVD apparatus (see below) for CNTs growth. The quality of carbon nanotube deposits on the gold catalyst were analyzed by using Atomic Force Microscopy (AFM), Scanning Electron Microscopy (SEM) and Raman spectroscopy.

## RESULTS AND DISCUSSION

Various plasma mixtures have been applied for CNTs growth up to date: Okita et al. have used a mixture of $H_2/CH_4$ [9], Gulas et al. have investigated gas phase kinetics of the CNT synthesis, by using different ratios of $NH_3/C_2H_2/H_2$ [3]. In the present study, three different mixtures of plasma $C_2H_2/H_2$, $N_2/C_2H_2/H_2$, $Ar/C_2H_2/H_2$ were used and the effects of each of them on the CNTs structure and morphological properties were comparatively analyzed.

The experimental results of this study have shown remarkable changes in diameter size, length, growth density and structural quality of the MWCNTs. In addition, the effect of plasma etching over the catalyst layer was investigated. The noticeable point is the growth temperature which was set on 550 $^{\circ}$C, lower in comparison to the growth temperature reported by others [39].

The XRD spectrum, Figure 1, indicates the structural details of the substrate used within this work. The three peaks, representing the structure of nickel, hcp (002) at 2Θ=42°, fcc (111) at 44.63° and fcc (200) at 2Θ=52.09° with the intensity of 1066.63, 333.69 and 9068.81, respectively, are evidenced. Therefore, according to this XRD pattern, the substrate is made of pure Ni, with more fcc structure.

Atomic force microscopy (AFM, XE-NSOM) was performed on the nickel substrate before and after the catalyst deposition, in contact mode on 3μm x 3μm area. Figure 2 shows 3D images and histograms of the topography versus the number of events for both types of the samples. The 3D images of the both samples show different topography, speaking about different average roughness for each sample. Therefore, as can be seen in Figure 2(a) and (c), the surface roughness for the pure nickel is much higher than for nickel coated by gold.

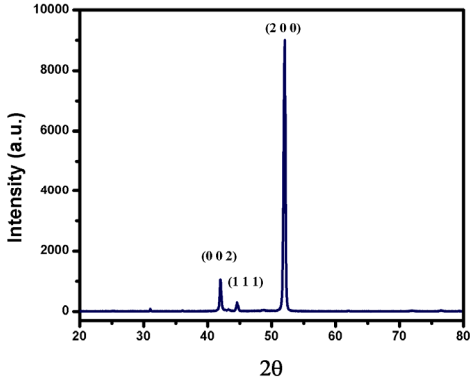


**Figure 1.** XRD pattern for the high purity nickel substrate

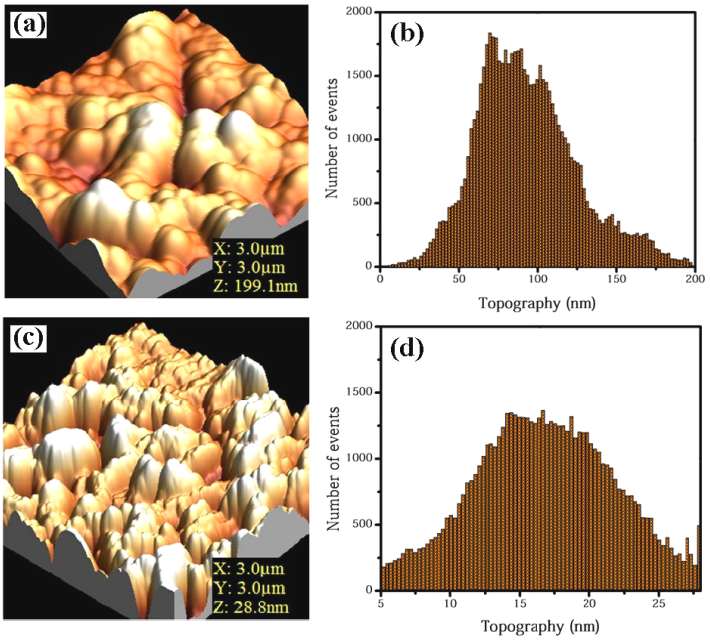


**Figure 2.** Three dimensional AFM images and histograms of the surface topography of: (a,b) pure nickel and (c,d) gold coated nickel substrate

The average roughness was found around 27.980 nm for the Ni substrate with no coatings. After gold coating, the morphology of the Ni surface was changed and the average roughness was reduced to 5.376 nm. As the Gaussian diagrams show, the homogeneity is lower for the pure nickel (Figure 2 (b)) than for the gold coated nickel substrate (Figure 2(d)).

The thickness of the gold nanolayer deposited on the nickel substrate as a catalyst by sputtering system was about 28.77 nm. Film thickness was measured using Rutherford back scattering (RBS) technique, using $He^+$ ion beam of 10μm in diameter, at 2.0 MeV. A typical RBS spectrum of Au thin film is given in Figure 3. The red line is obtained from exprimental data while the blue one is related to simulated data. The peak in the channel range of 310 to 340 indicated Au in the sample.

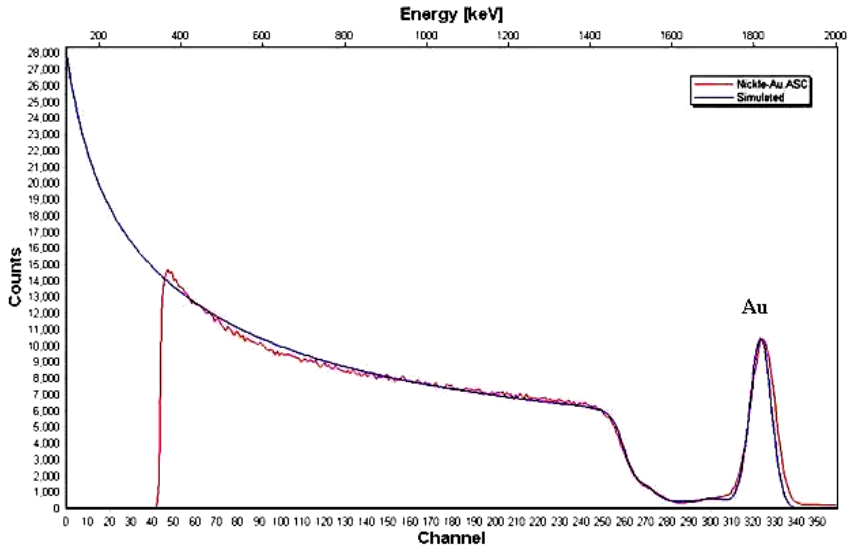


**Figure 3**. RBS curve shows the thicknesses of Au thin film deposited on nickel substrate

The SEM micrographs for the CNTs of the samples grown at different gase mixtures are shown in Figure 4. The range of CNTs diameter size, observesed in SEM images were analyzed statisticaly. The results are shown as a bar graphs in Figure 5. The red rectangular marks on the bars indicate the average diameter. Therefore, according to the bar graphs, the most disperse diameter size belongs to the samples $S_1$ and $S_2$, with the averege of 53 and 85 nm, respectively.

Adding $N_2$ gas to the plasma in the growth step resulted in new walls added to CNTs instead of growth in axial direction and length, so it has the maximum average among the other samples. The smalest bar graph belongs to the sample $S_3$. It means that adding Ar gas to the plasma in the growth phase, the diameter of CNTs and diversity in the size were dropped. The average in the sample $S_3$ is 23 nm although it had the lowest growth density on the surface, according to Figure 4. The last bar graph is referred

to $S_4$, of which size diversity is less than that of $S_1$ while the averege diameter decreased from 53 nm to 43.5 nm, more probably due to the lack of the etching step.

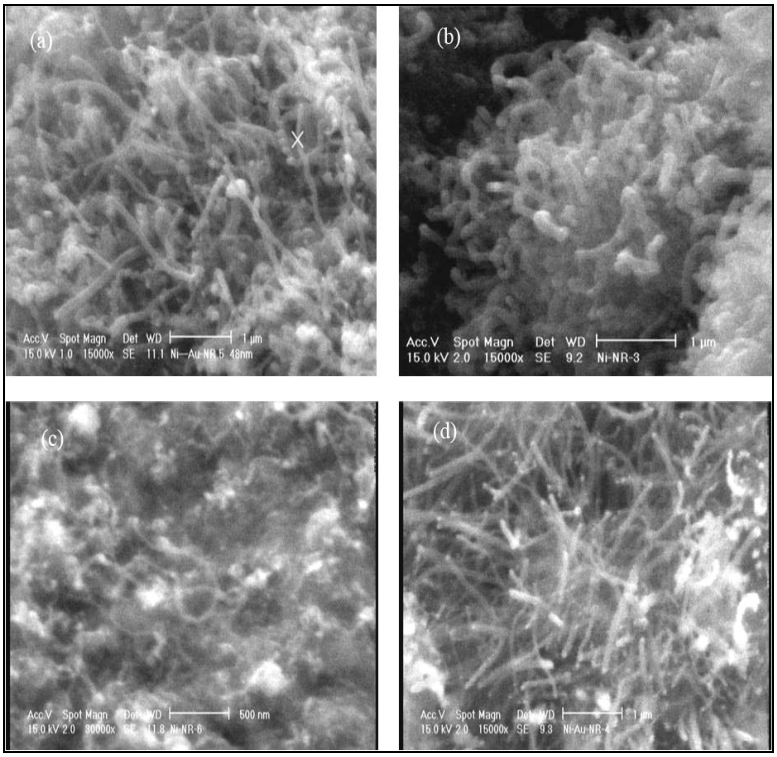


**Figure 4.** SEM micrographs show the effect of the dilution gases on CNTs growth: (a) $S_1$: $H_2$ ,(b) $S_2$: $H_2$/ $N_2$, (c) $S_3$: $H_2$/ Ar, (d) $S_4$: $H_2$ without plasma etching process

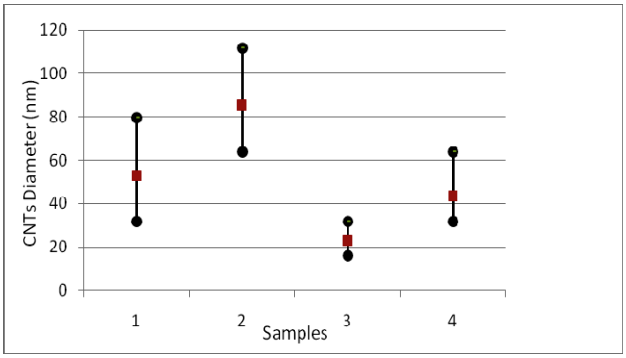


**Figure 5.** The bar graphs show the range of CNTs diameter size on the samples, the red rectangular marks indicating the average diameter.

Raman spectroscopy is widely used for the characterization of CNTs and the origins of the Raman bands seem to be well understood [40, 41]. The Raman spectra of the four samples are shown in the Figure 6; they are recorded on samples without purification. The peak around 1600 $cm^{-1}$ is related to the stretching mode in the graphite plane, in the CNTs axial direction, which is called the G-band. The other wide peak, related to the D-band longitudinal optical phonon, is around 1350 $cm^{-1}$ that is attributed to the pores or other defects in the $sp^2$ carbon structure. The G and D bands of samples $S_1$ and $S_2$ were observed at 1597 $cm^{-1}$ and 1354 $cm^{-1}$, respectively. These values were shifted to 1586 $cm^{-1}$ and 1342 $cm^{-1}$ in the sample $S_2$. The related peaks for $S_3$ were observed at 1600 $cm^{-1}$ and 1357 $cm^{-1}$. Therefore, the results show the plasma species in the growth step have influence on peaks position.

The ratio of D-band to G-band intensities $I_D/I_G$ is an important factor to analyze the quality of CNTs structure, whatever this value is less than one the non-defect graphene structure is much than the disorder structure and amorphus carbon in the sample. The lower $I_D/I_G$ values, of 0.967 and 0.968 are related to the sample $S_1$ and $S_2$, respectively. Although the CNT deposit appearance of the two above samples differs in diameter size, length and growth density, they have quite the same structural quality. For the sample $S_3$ the ratio was incresed to 0.976 but the difference is just 0.01. Finaly, the maximum ratio value, of 1.026, belongs to the sample $S_4$ so the effects of plasma etching process on the Au catalyst layer is obvious in the quality of CNTs structure.

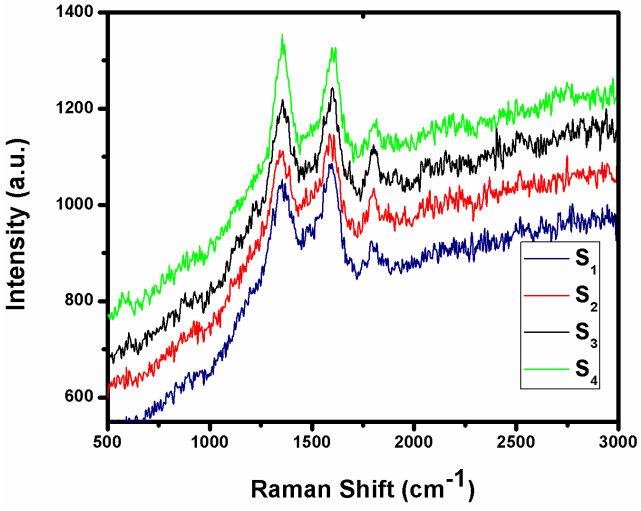


**Figure 6.** Raman spectra of the carbon nanotubes synthesized on gold coated nickel substrate: $S_1$ to $S_4$

We calculated the ratio $L_a=44/(I_D/I_G)$ to evaluate the CNTs quality. The results are 45.501, 45.454 and 45.082, for the samples $S_1$, $S_2$ and $S_3$ respectively. The value for $S_4$ is decreased to 42.885, therefore the effect of $H_2$ plasma etching treatment is clear here.

## CONCLUSIONS

In this paper, the effects of hydrogen etching gas and different gas mixtures were investigated. Using the gold nanolayer catalyst, enabled the carbon nanotube growth at relatively low temperature (550 °C) and with a high quality. Using the hydrogen etching gas favored the Au thin film reductions and created suitable sites for nanotubes tip growth. The SEM and Raman spectroscopy have shown that the CNTs grown by $H_2$ /$C_2H_2$ plasma $S_1$ have the highest quality, with lower $I_D/I_G$= 0.967 and the average diameter size about 53 nm. The next one is $S_2$ with $I_D/I_G$= 0.968, however this mixture of plasma increased the diameter size to 85 nm. In $S_3$ the average diameter size decreased to 23 nm. In addition, the ratio of $I_D/I_G$ increased to 0.976 and the density growth on the surface was remarkably decreased. In conclusion, by using suitable etching gas, good catalyst layer and relevant gas mixture, resulted in production of high quality carbon nanotubes.

## EXPERIMENTAL DETAILS

Pure wafer of nickel (Ni) with 1 mm thickness was used as substrate in 5×5 $mm^2$ surface dimension. The substrate was cleaned with acetone, ethanol and deionized water in an ultrasonic bath 15 min for each step and then was dried in air. Structure characterization of the substrate was performed by X-ray diffraction instrument (Siemens -D500 XRD). Atomic Force Microscopy (AFM-Park Scientific Instruments Auto Probe CP) was used to determine the substrate morphology in this step.

The cleaned substrate was transferred to a DC-sputtering system for catalyst coating. A thin film of gold (Au) with 28.77 nm thickness was coated on the Ni substrate in Ar plasma. In this step, AFM was used to compare the surface topography of the pure one and the other after catalyst layer deposition. Rutherford back scattering (RBS) analysis was applied to measure the layer thickness.

Plasma Enhanced Chemical Vapor Deposition system, manufactured by our group in Plasma Physics Research Center (PPRC), was applied for CNT growth (Figure 7). The coated substrate was put in the DC-PECVD reactor. The chamber was evacuated to $10^{-5}$ Torr and then, in the presence of $H_2$, the substrate was heated up to 550°C. The temperature was kept fix during the etching and growth processes. Etching processes performed by $H_2$ plasma. A mixture of $C_2H_2/H_2$ was used as carbon source and dilution gas. We investigated the gas mixture effects on CNTs growth by adding Ar and $N_2$ to the reactor in the growth process step. The experimental conditions are listed in Table 1.

**Table 1.** Experimental conditions for the carbon nanotubes growth on gold coated Ni substrate

| Sample No. | Etching gas | $P_{etching}$ (Torr) | Gas Mixture | Flow ratio | $P_{growth}$ (Torr) | $t_{growth}$ (min) |
|---|---|---|---|---|---|---|
| $S_1$ | $H_2$ | 2.5 | $C_2H_2$ / $H_2$ | 35/140 | 5 | 20 |
| $S_2$ | $H_2$ | 2.5 | $C_2H_2$ / $H_2$ / $N_2$ | 35/70/70 | 5 | 20 |
| $S_3$ | $H_2$ | 2.5 | $C_2H_2$ /$H_2$/ Ar | 35/70/70 | 5 | 20 |
| $S_4$ | - | - | $C_2H_2$ / $H_2$ | 35/140 | 5 | 20 |

Second harmonic of a Nd:YLF laser with 532 nm wavelength was used for Raman spectroscopy. SEM (XL30, Phillips, Holland) was used to determine the morphology and diameter estimates of the carbon nanotube deposits.

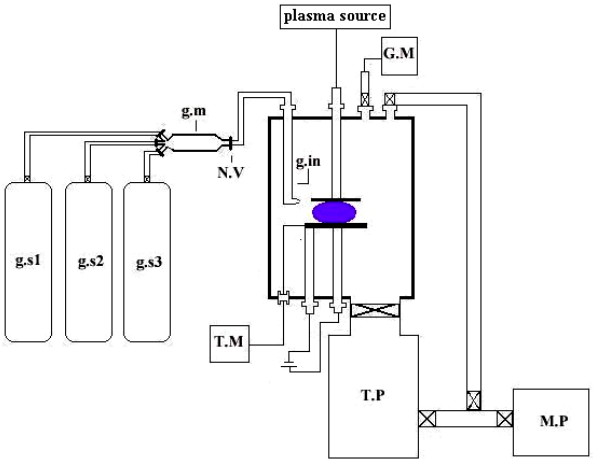


**Figure 7.** Schematic of the PECVD system manufactured by Plasma Physics Research Center.

## REFERENCES

1. Yong Seob Park, Eun Chang Choi, Byungyou Hong, *Applied Surface Science*, **2009**, *255*, 6028.
2. H. Sato et al., *Vacuum*, **2009**, *83*, 515.
3. M. Gulas, F. Le Normand, P. Veis, *Applied Surface Science*, **2009**, *255*, 5177.
4. H. Yoshida et al., *Nano Lett.*, **2009**, *9*, 3810.
5. J.K. Radhakrishnan et al., *Applied Surface Science*, **2009**, *255*, 6325.

6. Yeau-Ren Jeng, Hua-Chiang Wen, Ping-Chi Tsai, *Diamond & Relat. Mater.,* **2009**, *18*, 528.
7. M.R. Maschmann et al., *Carbon*, **2007**, *45*, 2290.
8. Duck-Hyun Lee et al., *Nanosci. Nanotechnol.,* **2008**, *8*, 5571.
9. A. Okita et al., *Carbon*, **2007**, *45*, 1518.
10. Y. Abdi et al., *Carbon*, **2008**, *46*, 1611.
11. F. Javier del Campo et al., *Electrochem. Commun*., **2008**, *10*, 1242.
12. I. Jang et al., *Carbon*, **2007**, *45*, 3015.
13. A. Chandrashekar et al., *Thin Solid Films*, **2008**, *517*, 525.
14. Ting Xu et al., *Materials Lett.*, **2009**, *63*, 867.
15. H. Ohno, *Surface Sci. Nanotechnol*., **2009**, *7*, 904.
16. Wei Fu et al., *Materials Res. Soc. Bull.,* **2004**, *845*, 223.
17. H.K. Patra et al., *Nanomedicine*, **2007**, *3*, 111.
18. G. F Paciotti et al., *Drug Delivery*, **2004**, *11*, 169.
19. S. Dhar et al., *Chem. Eur. J.,* **2008**, *12*, 10244.
20. J. Nam et al., *J. Am. Chem. Soc.*, **2009**, *131*, 13639.
21. N.P. Praetorius, T.K. Mandal, *Rec. Pat Drug Deliv. Formul*., **2007**, *1*, 37.
22. P. Chandra et al., *Digest J. Nanomater. Biostruct.*, **2010**, *5*, 363.
23. Z. Krpetic et al., *Gold Bull*., **2006**, *39*, 66.
24. In-Cheol Sun et al., *Chem. Eur. J*., **2009**, *15*, 13334.
25. Xiangyang Shi et al., *Small*, **2007**, *3*, 1245.
26. Seong Chu Lim et al., *NANO*, **2007**, *2*, 69.
27. Won Bong Choi et al., *Jpn. J. Appl. Phys*, **2000**, *39*, 2560.
28. A. Okazaki et al., *Jpn. J. Appl. Phys*, **2000**, *39*, 7067.
29. A. Javey et al., *Nature*, **2003**, *424*, 654.
30. O.E. Alon, *Phys. Rev. Lett*., **2000**, *85*, 5218.
31. A. Modi et al., *Nature*, **2003**, *424*, 171.
32. A.R. Harutyunyan et al., *Eur. Cells Mater*., **2002**, *3*, 84.
33. Zhuang Liu, Kai Chen, C. Davis et al., *Cancer Res.*, **2008**, *68*, 6652.
34. V.I. Merkulov et al., *Appl. Phys. Lett*., **2001**, *79*, 2970.
35. A. Gohier et al., *Carbon*, **2008**, *46*, 1331.
36. S. Iijima, *Nature*, **1991**, *354*, 56.
37. E. Vaghri, Z. Khalaj, M. Ghoranneviss, M. Borghei, *J. Fusion Energ*., **2011**, *30*, 447.

38. Z. Khalaj, M. Ghoranneviss, E. Vaghri, A. Saghaleini, M.V. Diudea, *Acta Chim. Slo*., **2012**, *59*, 338.

39. Ch. Taschner et al., *Surf. Coat. Technol*., **2003**, *81*, 174–175.

40. J.-Ph. Tessonnier et al., *Carbon*, **2009**, *47*, 1779.

41. J. Maultzsch, S. Reich, C. Thomsen, *Phys. Rev. B*, **2002**, *65*, 115.